New insights on the prevalence of drizzle in marine stratocumulus clouds based on a machine learning algorithm applied to radar Doppler spectra

6   Zeen Zhu[1], Pavlos Kollias[1,2], Edward Luke[1] and Fan Yang[1]

8   [1] Environmental and Climate Sciences Dept, Brookhaven National Laboratory Upton, NY, USA

9   [2]School of Marine and Atmospheric Sciences, Stony Brook University, Stony Brook, NY, USA

11   *Correspondence to:* Zeen Zhu (zeen.zhu@stonybrook.edu)

Abstract

15   The detection of the early growth of drizzle particles in marine stratocumulus clouds is important

16   for studying the transition from cloud water to rainwater. Radar reflectivity is commonly used to

17   detect drizzle; however, its utility is limited to larger drizzle particles. Alternatively, radar Doppler

18   spectrum skewness has proven to be a more sensitive quantity for detection of drizzle embryos.

19   Here, a machine-learning (ML) based technique that uses radar reflectivity and skewness for

20   detecting small drizzle particles is presented. Aircraft in-situ measurements are used to develop

21   and validate the ML algorithm. The drizzle detection algorithm is applied to three Atmospheric

22   Radiation Measurement (ARM) observational campaigns to investigate the drizzle occurrence in

23   marine boundary layer clouds. It is found that drizzle is far more ubiquitous than previously

24   thought, the traditional radar reflectivity-based approach significantly underestimates the drizzle

25   occurrence, especially in thin clouds with liquid water path lower than 50 $\mathrm{gm^{-2}}$. Furthermore, the

26   drizzle occurrence in marine boundary layer clouds differs among three ARM campaigns,

27   indicating that the drizzle formation which is controlled by the microphysical process is regime

28   dependent. A complete understanding of the drizzle distribution climatology in marine

29   stratocumulus clouds calls for more observational campaigns and continuing investigations.

30

31

1.Introduction

Clouds play an important role in the climate system and the accurate representation of their properties and feedbacks in Global Circulation Models (GCM) is essential for performing reliable future climate prediction (Cess et al., 1989;Bony et al., 2006;Vial et al., 2013). Among all the cloud types, marine stratocumulus is an important cloud type covering approximately 20% of the Earth's surface (Warren et al., 1986, 1988;Wood, 2012). Marine stratocumulus clouds significantly modulate the Earth's energy budget: on one hand, stratocumulus with high albedo strongly reflect incoming solar radiation back to space; on the other hand, as stratocumulus clouds have similar temperature with surface, they emit comparable amount of longwave radiation as the surface and do not significantly affect the infrared radiation emitted to space. Thus, overall the stratocumulus have a strong cooling effect to the climate system. (Hartmann et al., 1992). It is estimated that only a small increase of the marine stratocumulus coverage can compensate for the increased temperature induced by the greenhouse gas effect (Randall et al., 1984). Despite the considerable influence on the climate, large uncertainties persist in the representation of marine stratocumulus in GCMs due to a lack of understanding of the cloud properties and the associated processes (Stephens, 2005;Klein et al., 2017). One important issue is the representation of the early stage of the transition from cloud water to rainwater, which is parametrized by the autoconversion process via different schemes (Kessler, 1969;Khairoutdinov and Kogan, 2000). A misrepresentation of the autoconversion process in GCM's can affect not only the hydrological cycle but also generate compensating errors in the aerosol-cloud interactions (Michibata and Suzuki, 2020).

The core component of autoconversion is the production and growth mechanisms of drizzle drops. Drizzle, by definition, refers to liquid droplets with a diameter between 40 μm and 500 μm (Wood, 2005a;Glienke et al., 2017;Zhang et al., 2021). Drizzle is frequently observed in the warm cloud system and can modulate the cloud spatial organization and the boundary layer structure in several ways: the drizzle production process tends to warm the cloud layer and stabilize the boundary layer, which reduces cloud top entrainment and produces thicker clouds (Wood, 2012;Nicholls, 1984;Ackerman et al., 2009); the coalescence process can reduce cloud droplet concentration and cause cloud precipitation (Wood, 2006); furthermore, drizzle also plays a critical role in the

63 formation of the open-cell pattern of stratocumulus (Wang and Feingold, 2009;Feingold et al.,

64 2010) and tends to promote the stratocumulus to cumulus transitions process (Paluch and

65 Lenschow, 1991;Yamaguchi et al., 2017).

66

67 Despite the importance role of drizzle plays on the marine bounday layer, a thorough

68 understanding of its existence is incomplete due to the detection limitation. Historically, in-situ

69 and remote sensing measurements have been used to detect drizzle in cloud (Leon et al.,

70 2008;Wood, 2005a;Wu et al., 2015;Yang et al., 2018;VanZanten et al., 2005). In-situ

71 microphysical probes can provide size-resolved microphysical properties, importantly, Drop Size

72 Distribution (DSD), from which drizzle drops can be easily identified according to their definition.

73 The disadvantage of in-situ observations is the limited datasets collected during field campaigns,

74 making it challenging to provide long term statistical analyses. Millimeter-wavelength radar,

75 commonly known as cloud radar, is widely used for cloud/drizzle detections (Kollias et al., 2007a).

76 The total received backscatter power of droplets is converted to radar reflectivity factor, which is

77 independent of the radar wavelength in the cloud/drizzle regime, and is proportional to the sixth

78 power of the diameter of the particles in the radar resolution volume[1]. Compared with cloud

79 droplets, drizzle drops have larger diameters, which produce greater reflectivity, and this signature

80 is widely used to differentiate cloud/drizzle signals. Different reflectivity thresholds, ranging from

81 -15dBZ to -20dBZ, have been applied in previous studies to identify drizzle existence (Frisch et

82 al., 1995;Liu et al., 2008;Comstock et al., 2004). Nevertheless, this reflectivity-based technique

83 has obvious drawbacks. As reflectivity is the summation of the backscattered power from all the

84 droplets in a radar volume, the reflectivity threshold can detect the presence of drizzle drops only

85 when their contribution to the total radar backscatter exceeds that of the cloud droplets. More

86 specifically, when cloud droplets dominate the reflectivity signal, even if drizzle drops exist, they

87 fail to be detected as the total reflectivity is usually lower than -20 dBZ; this indicates that the

88 reflectivity-based technique is unable to detect small drizzle particles (Kollias et al., 2011b).

89

90 Besides reflectivity, another radar observed quantity which is sensitive to the presence of drizzle

91 is the skewness of the radar Doppler spectrum (hereafter skewness). Skewness is the third moment

92 of the radar-observed Doppler spectrum and is a measure of the asymmetry of the spectrum. For

---

[1] It is noted that attenuation is not considered in this study.

93 cloud droplets, Doppler spectra are on average symmetric with skewness equal to zero; as drizzle

94 drops grow and start falling, their terminal velocity is recorded in the fast-falling part of the

95 Doppler spectra, which has greater backscatter power than the power contributed by cloud droplets,

96 leading to asymmetric spectra with a non-zero skewness (Kollias et al., 2011b;Luke and Kollias,

97 2013). The capability of using skewness to detect early drizzle development stages was

98 demonstrated in Acquistapace et al. (2019), where a skewness threshold as 0.379 was estimated

99 from the Doppler skewness time series standard deviation based on the carefully selected

100 nondrizzling clouds(Acquistapace et al., 2017). Considering the noisiness in the estimation of the

101 third moment of the radar Doppler spectrum, the use of a fixed threshold value may lead to

102 considerable misclassifications. Here, a supervised Machine Learning (ML) algorithm is used to

103 provide a more robust detection of drizzle particles in warm stratiform clouds. First, in-situ DSD

104 measurements are used as input to a sophisticated radar Doppler spectrum simulator that can

105 accurately represent the performance of the ARM profiling cloud radars in estimating the

106 corresponding radar-observed reflectivity and skewness. Next, the ML algorithm is trained from

107 2 months of in-situ observations to generate a classification model; the classification results from

108 one case study will be presented and compared against the in-situ measurements. Finally,

109 comprehensive datasets from three ARM observational campaigns are used to investigate drizzle

110 occurrence and demonstrate the omnipresence of drizzle in marine stratocumulus clouds.

111

112 **2.Instruments and Data**

113

114 The data used in this study are collected from three observatories operated by the U.S. Department

115 of Energy's Atmospheric Radiation Measurement (ARM) facility. The Eastern North Atlantic

116 (ENA) is a permanent observational site established on Graciosa Island in the Azores archipelago

117 in 2013 as representative of a maritime environment. The Aerosol and Cloud Experiments in the

118 Eastern North Atlantic (ACE-ENA) field campaign was conducted in the vicinity of the ENA site

119 from June 2017 to February 2018. The Gulfstream-1 aircraft was deployed during ACE-ENA to

120 provide in-situ measurements. The Marine ARM GPCI Investigation of Clouds (MAGIC)

121 campaign was based on a mobile observatory facility traversing between Los Angeles, California,

122 and Honolulu, Hawaii, from October 2012 to September 2013. Measurements of Aerosols,

123 Radiation, and Clouds over the Southern Ocean (MARCUS) was a field campaign conducted from

October 2017 to April 2018 along the route between Hobart, Australia, and the Antarctic. All of the observational campaigns were equipped with a variety of instruments which provide comprehensive datasets being used in this study.

The primary instrument being used in this study is the cloud radar: a Ka-Band ARM Zenith Radar (KAZR) was operated at ENA and MAGIC and a W-Band ARM Cloud Radar (WACR) was used during MARCUS. The KAZR and WACR are both vertically pointing with 30 m range resolution; the temporal resolution of the WACR and KAZR used at ENA is 2 s, while the temporal resolution of the KAZR used for MAGIC is 0.36 s. To make the observations comparable, radar moments from MAGIC are averaged over 2 s to be consistent with the ones collected at ENA and MARCUS. Radar reflectivity and Doppler skewness are obtained from the Microscale Active Remote Sensing of Clouds (MicroARSCL) product (Kollias et al., 2007b). Radar reflectivity at ENA and MAGIC is calibrated with surface-based measurements of the raindrop PSD using a disdrometer (Gage et al., 2000;Kollias et al., 2019). At MARCUS, a disdrometer is not suitable for radar calibration thus instead we follow Mace et al. (2021) by adding 4.5 dB to the reflectivity for WACR calibration. In addition, a ceilometer and microwave radiometer (MWR) are used to estimate cloud base height and liquid water path (LWP). The time resolution of the MWR and ceilometer are 10 s and 15 s respectively. Besides the surface-based observations, in-situ measurements from ACE-ENA during the intensive observation period 1 (IOP1) which was conducted from 21 June to 20 July in 2017 are also used in this study. The DSD of hydrometeors with diameter ranging from 1.5 μm to 9075 μm are characterized using combined measurements from the fast cloud droplet probe (FCDP), 2-dimensional stereo probe (2D-S) and high-volume precipitation spectrometer (HVPS-3). Liquid water content is measured using a multi-element water content system and a Gerber probe.

3.Methodology

As Doppler skewness is a sensitive indicator of weak drizzle signals, the focus of the methodology is to synthesize this quantity with reflectivity to construct a robust drizzle detection algorithm. Thus, the key issue lies in the challenging task of determining the appropriate reflectivity/skewness combination to identify drizzle signals. Here we address this problem in a novel way: first we

155 identify the existence of cloud/drizzle based on in-situ observed DSDs; then a well-established
156 Doppler spectrum simulator is applied to emulate the radar observed spectrum for the given DSD
157 and estimate the corresponding reflectivity and skewness. Finally, a machine learning algorithm
158 is trained by the collection of well-defined cloud/drizzle datasets to resolve the drizzle
159 identification function.
160

161 **3.1 Doppler spectrum simulation**

162

163 According to previous studies, liquid droplets with diameter exceeding 40 μm are defined to be
164 drizzle (Wood, 2005a;Zhang et al., 2021). We follow this definition to classify the in-situ observed
165 DSD: cloud/drizzle are defined by the maximum diameter in the DSD being smaller/larger than
166 40 μm. Example DSDs of cloud-only and mixed cloud-drizzle conditions are shown in Fig. 1a and
167 Fig. 1c. Next, the Doppler spectrum simulator developed by Kollias et al. (2011a) is applied to
168 generate the radar-observed Doppler spectrum based on the in-situ DSD. The associated simulator
169 parameters are set as follows: Doppler spectra are generated with 256 FFT bins and a Nyquist
170 velocity of $\pm$6 m/s, which correspond to the KAZR configuration operated by ARM (Kollias et
171 al., 2016); turbulence broadening (σ_t) is set as 0.2m/s which is obtained from local observations.
172 For the vertical pointing radar, the observed spectrum width is a measure of the Doppler spectrum
173 broadening which is mainly contributed by three factors: turbulence (σ_t), microphysics (i.e., the
174 falling velocity difference among hydrometers with different size) and the wind shear effects
175 (usually is negligible compared to other two terms). (Borque et al., 2016) In our study, we assume
176 that in the non drizzling or weakly drizzling clouds, Doppler spectral broaden is mainly contributed
177 by the turbulence factor, thus the observed second-moment of the Doppler spectrum, i.e. spectrum
178 width, can be directly used to indicate the turbulence broadening factor (σ_t). The mean value of
179 KAZR-observed spectrum width collected from the ACE-ENA IOP1 is estimated as 0.2 m/s (Fig.
180 S1). Thus, σ_t is selected as 0.2m/s for the Doppler spectrum simulator to represent the typical
181 turbulence environment for the stratocumulus clouds of interest. Finally, radar noise is simulated
182 by adding random perturbation to the Doppler spectra; positive velocity indicates downward
183 motion. A detailed description of the Doppler spectrum simulator application is found in Zhu et al.
184 (2021). Once a spectrum is generated, a post-processing algorithm (Kollias et al., 2007b) is used
185 to eliminate noise (Hildebrand and Sekhon, 1974) and to estimate the Doppler moments, i.e.

186 reflectivity and skewness. To demonstrate that the simulator can represent radar observations, the
187 simulated reflectivity and skewness are compared with KAZR observations (Fig. S2) and shows
188 consistent ranges and distribution pattern, indicating that the simulated radar moments are capable
189 to represent the real observation signal. The relatively large fraction of the in-situ measurements
190 with dBZ > -20 in Fig. S2 is likely caused by the different observational strategies between in-situ
191 and KAZR measurements (Wang et al., 2016).

192

193 Fig. 1b and 1d show examples of the simulated Doppler spectra along with the estimated
194 reflectivity and skewness for a cloud-only and mixed cloud-drizzle DSD. It is noticed for the
195 drizzle case (Fig. 1d), reflectivity is well below the conventional threshold (-20 ~ -15 dBZ) used
196 for drizzle detection and is unable to discriminate it from the cloud-only case (Fig. 1b). Skewness,
197 however, shows a significant difference between drizzle (0.5) and cloud (0), emphasizing the
198 importance of including skewness as an additional indicator for drizzle detection.

199

3.2 Machine Learning algorithm application

201

202 From the IOP1 of ACE-ENA, 6000 in-situ observed DSDs (2000 for cloud-only and 4000 for
203 mixed cloud-drizzle) are selected from the cloudy samples defined as having liquid water content
204 larger than 0.01 gm^{-3} (Zhang et al., 2021). For each DSD, the spectrum simulator is applied to
205 estimate the reflectivity and Doppler skewness. The distribution of these two quantities for all the
206 selected datasets is shown in Fig. 2. It shows that drizzle with positive skewness tends to be
207 associated with reflectivity lower than -20 dBZ. For reflectivity ranging from -35 to -25 dBZ and
208 skewness around zero, the drizzle signal overlaps with cloud; this region represents the early stage
209 of drizzle initiation with low reflectivity and indistinguishable skewness features compared with
210 cloud signals.

211

212 In order to determine the classification boundary to distinguish cloud/drizzle categories (i.e.
213 red/blue points in Fig. 2), we apply a supervised machine learning algorithm which is widely used
214 in classification-related problems, the Support Vector Machine (SVM) (Cortes and Vapnik,
215 1995;Vapnik et al., 1997). SVM handles complicated data classification tasks by solving
216 optimization relationships and finding the optimal classification equations in the feature space.

217 There are three reasons to use SVM in this study: 1) SVM is nonparametric and thus does not

218 require specification or assumption of the classification equation; 2) By applying the appropriate

219 kernel, SVM can generate a non-linear classification boundary to classify non-linearly separable

220 datasets; 3) The decision boundary resolved by SVM will separate the categories with maximum

221 distance; this is a distinctive feature of the SVM algorithm which is extensively used in a variety

222 of areas (Ma and Guo, 2014).

223

224 For the collected cloud/drizzle datasets, 80% of them are used for training, and the remain 20%

225 for validation. Inputs to the SVM are Doppler skewness and reflectivity, where the reflectivity

226 from -50 dBZ to 0 dBZ is normalized from -1 to 0; the output is classified as either cloud (0) or

227 drizzle (1). Here the Radial Basis Function (RBF) with two tuning parameters, Γ and C, is used as

228 the SVM kernel (Keerthi and Lin, 2003). The RBF kernel is one of the most widely used kernels

229 due to its similarity to the Gaussian distribution. The Γ parameter determines the curvature of the

230 decision boundary with a high value indicating more curvature for capturing the complexity of the

231 dataset; C is a regularization parameter to set the classification accuracy versus the maximization

232 of the decision function margin; a lower C leads to a larger margin, and a simpler decision function

233 at the cost of training accuracy. Following Davis and Goadrich (2006), we use precision/recall to

234 evaluate the performance of the classification outcome. In this study, precision refers to the number

235 of correct drizzle detections divided by total drizzle detections reported by the SVM, and recall

236 refers to the number of the correct drizzle detections divided by the number of true drizzle

237 occurrences in dataset. Different combinations of RBF parameters with Γ ranging from 1 to 500

238 and C from 1 to 1000 are applied, with the classification outcome shown in Table 1. Besides using

239 the metrics as recall/precision, the shape of the resolved boundary is also examined visually to

240 avoid the ML algorithm being overfitted. As shown in Fig. S3 ~ Fig. S8, parameter with large C

241 and Γ leads to better classification outcome but will cause overfitting issues. Here we choose $\Gamma =$

242 50 and C = 1 as the preferred parameters to produce classification results with precision and recall

243 as 98% and 85%, respectively. That is, for the cloud-drizzle dataset collected at ACE-ENA, at

244 most, 85% of the drizzle can be detected by the algorithm and among the detection outcomes, 98%

245 are true drizzle signals.

246

247 The resolved classification boundary is shown as the black line in Fig. 2. We can see the algorithm
248 reasonably separates the cloud/drizzle clusters; the resolved skewness threshold being used to
249 distinguish cloud/drizzle is around ± 0.2, and the maximum reflectivity used for classification is -
250 20dBZ. These values are consistent with previous studies (Frisch et al., 1995;Liu et al.,
251 2008;Kollias et al., 2011b;Acquistapace et al., 2019). We further estimate the cumulative
252 distribution function (CDF) of the correctly detected drizzle samples as a function of dBZ from
253 the ML technique (magenta solid line in Fig. 2) and from the traditional method with reflectivity
254 threshold ranging from -20 to -15 dBZ. (magenta shading in Fig. 2). It is noticed that drizzle can
255 be detected with dBZ <-30 from the ML method; this value is significantly lower than for
256 traditional thresholds in use. The ML method is more sensitive to the weak drizzle signals than the
257 dBZ thresholds that have been proposed. Specifically, compared to the ML technique, 35% and
258 21% of the drizzle are missed by the reflectivity threshold approach when using dBZ >-20 and
259 dBZ >-15, respectively. Another important implication of this result is that dBZ >-15 is
260 traditionally applied by CloudSat to identify light rain incidence (Haynes et al., 2009); here we
261 demonstrate that a more robust threshold is likely to be much lower. A more detailed performance
262 comparisons of the two drizzle detection methods are shown in Fig. S9, where the results are
263 similar with Fig.2, the rise of the false detection rate for the ML-based method for reflectivity
264 lower than -20dBZ is due to the exists of the extremely weak drizzle signals as will be discussed
265 later.
266
267 Besides the encouraging performance of the ML technique, some noticeable issues can be
268 identified: 1) Compared with the true CDF of the drizzle fraction (dotted magenta line in Fig. 2),
269 20% of drizzle is undetected. This missing drizzle subset, as explained previously by the
270 overlapping area, is composed of tiny drizzle embryos that have yet to develop distinctive features
271 compared with their cloud counterparts. 2) Another issue is the unrealistic broadening of the
272 classification boundary for reflectivity lower than -35dBZ; this issue is related to the kernel being
273 applied in the SVM algorithm. Since drizzle rarely exists below -35 dBZ, this issue will not affect
274 the classification performance as far as we are concerned.
275
276
277

4.Results

The ML-based drizzle detection algorithm is applied to the dataset collected at three ARM observatories. First, an example case is presented for which aircraft observations are available and the corresponding in-situ measurements are used to demonstrate the performance of the algorithm. Then, the drizzle occurrence on classified stratocumulus clouds at ENA, MARCUS and MAGIC observatories are presented; the differences of the drizzle occurrence from the proposed machine learning based algorithm (hereafter MLA) and the traditional dBZ-based algorithm (hereafter dBZA) are compared to indicate that drizzle occurrence in stratocumulus clouds is far more frequent that has been previously suggested. For the dBZA, we use reflectivity >-17 dBZ for drizzle identification, while the application of other thresholds ranging from -20 to -15 dBZ did not affect the results as discussed.

4.1 Single cloud layer case

For the selected case (Fig. 3), a thin cloud layer with thickness around 150m is identified. Cloud signals is very weak with 99% of reflectivity lower than -17 dBZ. However, considerable large skewness values shown in Fig. 3b indicates the presence of the drizzle particles. The classification results from the MLA classification are shown in Fig. 3c, it can be seen that drizzle is omnipresent and spread throughout the cloud layer, mixed with cloud-only detections.

Here the in-situ observed DSD is used to verify the MLA detection. On June 30th, 2017, aircraft measurements were conducted from 09:27 to 13:16 UTC. We constrained the in-situ measurements to be within 20 km of the ENA observatory (Fig. 4). Considering that the average in-cloud wind speed is 3.7 m/s, the distance of 20 km is equivalent to around 1.5 hour of KAZR observations; thus, the radar measurements from 08:00 to 13:30 UTC are selected to match the aircraft observations. We assume the signal of the drizzle/cloud occurrence collected from the in-situ measurements can be used to verify the drizzle presence observed from KAZR. For the selected period, drizzle occurrence is 47% from the MLA detections and 65% from the in-situ observations. The 18% of the missing drizzle by MLA is largely attributed to the "overlapping area" shown in Fig. 2 indicating the early stage of drizzle embryos which are indistinguishable

309   from cloud droplets. Nevertheless, this comparison provides strong evidence that drizzle is widely

310   present in the cloud layer for the selected case and demonstrates that the classification results from

311   MLA are reliable. Contrastingly, negligible drizzle signals (0.05%) are detected with the

312   reflectivity-based (dBZ >-17) technique.

313

314   **4.2 Drizzle occurrence at ARM campaigns**

315

316   During the operational periods of ACE-ENA, MARCUS and MAGIC, single-layer marine

317   stratocumulus clouds are selected with cloud top temperature greater than 0 °C and cloud top

318   height lower than 4000 m. The moving standard deviation of cloud top height within 30-minutes

319   (σ) is calculated and profiles with σ larger than 200 m are excluded to reject non-stratocumulus-

320   type clouds. LWP retrievals are biased when MWR is wet; thus, radar profiles with their lowest

321   range gates containing hydrometeor detections are considered to be precipitation and are removed

322   from the analysis. A complete list of the days being used is shown in Table 2. In total, 204, 72, and

323   215 hours of radar observation were selected from the ACE-ENA, MARCUS and MAGIC

324   campaigns.

325

326   In order to composite cloud layers with different thickness, cloud height is normalized between 0

327   to 1 as:

$$h = \frac{H - H_b}{H_t - H_b}$$

328

329

330   Where H is the physical height of a given radar gate, H_t and H_b is the cloud top and base height.

331   h=0 represents cloud base and h=1 indicates cloud top.

332

333   Drizzle occurrence is calculated as the number of drizzle detections divided by the total observed

334   signals in each normalized height bin (0.1) and LWP bin (50 g m^{-2}). The drizzle occurrence being

335   detected from both methods at the three ARM observatories are shown in Fig. 5. For all the

336   observational site/campaigns, drizzle is more likely to occur as LWP increases. This tendency

337   holds true despite the drizzle detection method being used. However, for each observational

338   campaign, drizzle occurrence detected from MLA (Fig. 5 a, b, c) is always larger than from dBZA

339 (Fig. 5 d, e, f). This difference becomes significant especially for thin clouds with low LWP: when

340 LWP is under 50 g m^{-2}, or equivalently, cloud thickness is less than 200 m (Fig. 6), drizzle

341 occurrence being detected from dBZA is around 0.1 while it is 0.4~0.5 from MLA. This result

342 clearly indicates that the traditional drizzle detection method based on a reflectivity threshold

343 significantly underestimates the true drizzle occurrence, especially in thin cloud layers. To

344 quantitatively describe the detection performance, we estimate the relative percentage difference

345 of the drizzle detections between two methods as follows:

346
$$P_{LWP} \ (\%) = \frac{N_{MLA,LWP} - N_{dBZA,LWP}}{N_{MLA,LWP}} * 100$$

347 Where $N_{MLA,LWP}$ and $N_{dBZA,LWP}$ indicate the number of the drizzle detection by MLA and dBZA

348 respectively for a given LWP category. The results (Fig. 7a) indicate that when LWP is smaller

349 than 50 g m^{-2}, which frequently occurs under the ENA and MAGIC campaigns (Fig. 7b), 90% of

350 drizzle are missed by dBZA at ENA and MARCUS, and 60 % of drizzle is undetected at MAGIC

351 compared with MLA. An application of a relative lower reflectivity threshold with dBZ< -20, to

352 some degree, mitigate the missing drizzle detections compared with MBL, but still with 50~80%

353 of the drizzle being undetected (shading area in Fig. 7a).

354

355 Besides the considerable drizzle signals missed by dBZA, another implication to be noted is the

356 difference of drizzle distribution among the three ARM campaigns. Specifically, large drizzle

357 fractions tend to occur in the upper part of cloud at ENA and in the lower parts of cloud at

358 MARCUS and MAGIC (Fig. 5). When compared with MLA, the missing drizzle detections based

359 on dBZA are much more significant for ENA/MARCUS than for MAGIC (Fig. 7a). The different

360 drizzle distribution pattern suggests that clouds among these three campaigns might have different

361 microphysical properties and processes that controls the drizzle initiation. For instance, the

362 contrasting thermodynamics environment among the ARM campaigns with low/high temperature

363 and humidity at MARCUS/MAGIC might leads to different autoconversion process which control

364 the drizzle formation. In particular, we suspect that a more humid environment under MAGIC will

365 benefits the generation of larger cloud droplets compared with the other campaigns (Laird et al.,

366 2000;Zhou et al., 2015). Fig. 8 supports this hypothesis by showing that the mean cloud reflectivity

367 at MAGIC is 8dB larger than it is at the other two campaigns for LWP smaller than 100 gm^{-2}. The

368 relatively large dBZ for small LWP, to some degree, mitigates the underrepresented drizzle
369 detection by the reflectivity-based method.
370
371 5.**Conclusion and Discussion**
372
373 Building on the concept that radar Doppler spectra skewness is more sensitive to drizzle presence,
374 a new method of detecting drizzle in marine boundary clouds is presented. In-situ observed DSDs
375 are used to unambiguously classify cloud and drizzle particles; then, a radar Doppler spectra
376 simulator is applied to estimate the expected radar-observed reflectivity and skewness. Extensive
377 datasets collected from the ACE-ENA campaign are trained via the ML-based algorithm to
378 optimally determine a classification equation of cloud/drizzle. The proposed algorithm is validated
379 by the in-situ measurements to successfully detect weak drizzle signals, which are completely
380 missed by the traditional reflectivity-based technique.
381
382 The drizzle/cloud classification outcome of a thin cloud layer observed on June 30, 2017 at ENA
383 was presented to show the performance of the detection algorithm. It was found that even for thin
384 cloud with thickness less than 150 m, a significant amount of drizzle already exists; this
385 classification result is further verified by the in-situ observations. Furthermore, a statistical
386 analysis compares the drizzle occurrence from two detection methods at the ACE-ENA, MARCUS
387 and MAGIC field campaigns. The results indicate that drizzle is ubiquitous in cloud layers and its
388 existence has been significantly underestimated by conventional reflectivity-based methods,
389 especially in thin cloud layers. The ubiquitous of drizzle in the MBL clouds calls for investigations
390 on the drizzle formation mechanism. It is known that the growth of liquid droplets by diffusion is
391 not efficient with radius larger than 20 μm, thus other mechanisms that favors drizzle formation
392 greatly contribute the drizzle existence. The presented results provide observational evidence to
393 verify the drizzle formation theories. The drizzle occurrence and vertical structure differ among
394 the three campaigns, indicating that drizzle formation and distribution in marine stratocumulus
395 clouds might be regime dependent, determined by microphysical and dynamical process in the
396 local region. In this study, data from the three observational campaigns are used to explore the
397 drizzle frequency of marine stratocumulus in middle/high latitude regions; however, it is quite
398 possible that the drizzle occurrence from other locations might differ from the presented results.

399 A complete understanding of the drizzle climatology in marine stratocumulus clouds calls for more

400 campaign observations and continuing investigations.

401

402 The results in this study provide a new perspective for viewing drizzle existence in radar

403 observations with the hope of shedding light on several critical topics in the warm cloud studies:

404 1) In most microphysics retrieval algorithms, the existence of drizzle particles is determined by a

405 reflectivity threshold. However, this study shows the presence of significant drizzle drops during

406 low reflectivity conditions (lower than -20 dBZ) and a lack of considering this may lead to a certain

407 degree of the retrieval uncertainty; 2) Drizzle production mechanisms are widely regarded as a

408 critical missing piece of the puzzle in warm cloud research (Takahashi et al., 2017). Particularly,

409 the parameterization schemes of the autoconversion/accretion processes in numerical models have

410 large variations among each other, leading to significant uncertainty in future climate predictions

411 (Michibata and Suzuki, 2020;Wood, 2005b). The results presented in this study can be used to

412 verify the proposed parameterization schemes by comparing the drizzle climatology. 3)

413 Furthermore, the novel utilization of in-situ and remote sensing synthesis of observations presented

414 in this study yields insights on the potential of combined multi-platform observations to investigate

415 the microphysical processes in warm clouds.

416

417

418

419

420
421
422 ***Data availability:*** The ARM observational datasets are available at the ARM Data Center. The
423 KAZR data (kazrge) can be accessed via http://dx.doi.org/10.5439/1025214. The ceilometer
424 dataset (ceil) can be accessed via http://dx.doi.org/10.5439/1181954. The retrieved LWP product
425 (mwrret2turn) can be accessed via http://dx.doi.org/10.5439/1566156. The in-situ observation
426 during the ACE-ENA campaign can be accessed via
427 https://adc.arm.gov/discovery/#/results/iopShortName::aaf2017ace-ena.
428
429

430 ***Supplement***: The supplement related to this article is available online at:
431

432

433 ***Author contributions***: Z.Z. designed the methodology and performed the analysis. P.K.
434 contributed the design of the study. E.L provide the MicroARSCL datasets. F.Y. assisted in the
435 interpretation of results. Z.Z. prepared the manuscript with contributions from all co-authors.
436

437 ***Competing interests:*** The authors declare that they have no conflict of interest.

438

439 ***Acknowledgments***: We would also like to acknowledge the data support provided by the
440 Atmospheric Radiation Measurement (ARM) Program sponsored by the U.S. Department of
441 Energy.

442

443 ***Financial support:*** Z. Z.'s contributions were supported by the U.S. Department of Energy (DOE)

444 ASR ENA Site Science award. P. K., E. L. and F. Y. were supported by the US Department of

445 Energy (DOE) Atmospheric System Research Program under contract DE-SC0012704.
446
447
448

References

Ackerman, A. S., VanZanten, M. C., Stevens, B., Savic-Jovcic, V., Bretherton, C. S., Chlond, A., Golaz, J.-C., Jiang, H., Khairoutdinov, M., and Krueger, S. K.: Large-eddy simulations of a drizzling, stratocumulus-topped marine boundary layer, Monthly Weather Review, 137, 1083-1110, 2009.

Acquistapace, C., Kneifel, S., Löhnert, U., Kollias, P., Maahn, M., and Bauer-Pfundstein, M.: Optimizing observations of drizzle onset with millimeter-wavelength radars, Atmospheric Measurement Techniques, 10, 1783-1802, 2017.

Acquistapace, C., Löhnert, U., Maahn, M., and Kollias, P.: A new criterion to improve operational drizzle detection with ground-based remote sensing, Journal of Atmospheric and Oceanic Technology, 36, 781-801, 2019.

Bony, S., Colman, R., Kattsov, V. M., Allan, R. P., Bretherton, C. S., Dufresne, J.-L., Hall, A., Hallegatte, S., Holland, M. M., Ingram, W., Randall, D. A., Soden, B. J., Tselioudis, G., and Webb, M. J.: How well do we understand and evaluate climate change feedback processes?, Journal of Climate, 19, 3445-3482, 10.1175/jcli3819.1, 2006.

Borque, P., Luke, E., and Kollias, P.: On the unified estimation of turbulence eddy dissipation rate using Doppler cloud radars and lidars, Journal of Geophysical Research: Atmospheres, 121, 5972-5989, 2016.

Cess, R. D., Potter, G., Blanchet, J., Boer, G., Ghan, S., Kiehl, J., Le Treut, H., Li, Z.-X., Liang, X.-Z., and Mitchell, J.: Interpretation of cloud-climate feedback as produced by 14 atmospheric general circulation models, Science, 245, 513-516, 1989.

Comstock, K. K., Wood, R., Yuter, S. E., and Bretherton, C. S.: Reflectivity and rain rate in and below drizzling stratocumulus, Quarterly Journal of the Royal Meteorological Society: A journal of the atmospheric sciences, applied meteorology and physical oceanography, 130, 2891-2918, 2004.

Cortes, C., and Vapnik, V.: Support-vector networks, Machine learning, 20, 273-297, 1995.

Davis, J., and Goadrich, M.: The relationship between Precision-Recall and ROC curves, Proceedings of the 23rd international conference on Machine learning, 2006, 233-240,

Feingold, G., Koren, I., Wang, H., Xue, H., and Brewer, W. A.: Precipitation-generated oscillations in open cellular cloud fields, Nature, 466, 849-852, 2010.

Frisch, A., Fairall, C., and Snider, J.: Measurement of stratus cloud and drizzle parameters in ASTEX with a Kα-band Doppler radar and a microwave radiometer, Journal of the Atmospheric Sciences, 52, 2788-2799, 1995.

Gage, K. S., Williams, C. R., Johnston, P. E., Ecklund, W. L., Cifelli, R., Tokay, A., and Carter, D. A.: Doppler radar profilers as calibration tools for scanning radars, Journal of Applied Meteorology, 39, 2209-2222, 2000.

Glienke, S., Kostinski, A., Fugal, J., Shaw, R., Borrmann, S., and Stith, J.: Cloud droplets to drizzle: Contribution of transition drops to microphysical and optical properties of marine stratocumulus clouds, Geophysical Research Letters, 44, 8002-8010, 2017.

Hartmann, D. L., Ockert-Bell, M. E., and Michelsen, M. L.: The effect of cloud type on Earth's energy balance: Global analysis, Journal of Climate, 5, 1281-1304, 1992.

Haynes, J. M., L'Ecuyer, T. S., Stephens, G. L., Miller, S. D., Mitrescu, C., Wood, N. B., and Tanelli, S.: Rainfall retrieval over the ocean with spaceborne W‑band radar, Journal of Geophysical Research: Atmospheres, 114, 2009.

Hildebrand, P. H., and Sekhon, R.: Objective determination of the noise level in Doppler spectra, Journal of Applied Meteorology, 13, 808-811, 1974.

Keerthi, S. S., and Lin, C.-J.: Asymptotic behaviors of support vector machines with Gaussian kernel, Neural computation, 15, 1667-1689, 2003.

Kessler, E.: On the distribution and continuity of water substance in atmospheric circulations, in: On the distribution and continuity of water substance in atmospheric circulations, Springer, 1-84, 1969.

Khairoutdinov, M., and Kogan, Y.: A new cloud physics parameterization in a large-eddy simulation model of marine stratocumulus, Monthly weather review, 128, 229-243, 2000.

Klein, S. A., Hall, A., Norris, J. R., and Pincus, R.: Low-cloud feedbacks from cloud-controlling factors: A review, Shallow Clouds, Water Vapor, Circulation, and Climate Sensitivity, 135-157, 2017.

Kollias, Clothiaux, E. E., Miller, M. A., Albrecht, B. A., Stephens, G. L., and Ackerman, T. P.: Millimeter-wavelength radars - New frontier in atmospheric cloud and precipitation research, Bulletin of the American Meteorological Society, 88, 1608-+, 10.1175/bams-88-10-1608, 2007a.

Kollias, Clothiaux, E. E., Miller, M. A., Luke, E. P., Johnson, K. L., Moran, K. P., Widener, K. B., and Albrecht, B. A.: The Atmospheric Radiation Measurement Program cloud profiling radars: Second-generation sampling strategies, processing, and cloud data products, Journal of Atmospheric and Oceanic Technology, 24, 1199-1214, 10.1175/jtech2033.1, 2007b.

Kollias, Remillard, J., Luke, E., and Szyrmer, W.: Cloud radar Doppler spectra in drizzling stratiform clouds: 1. Forward modeling and remote sensing applications, Journal of Geophysical Research-Atmospheres, 116, 10.1029/2010jd015237, 2011a.

Kollias, Szyrmer, W., Remillard, J., and Luke, E.: Cloud radar Doppler spectra in drizzling stratiform clouds: 2. Observations and microphysical modeling of drizzle evolution, Journal of Geophysical Research-Atmospheres, 116, 10.1029/2010jd015238, 2011b.

Kollias, Clothiaux, E. E., Ackerman, T. P., Albrecht, B. A., Widener, K. B., Moran, K. P., Luke, E. P., Johnson, K. L., Bharadwaj, N., and Mead, J. B.: Development and applications of ARM millimeter-wavelength cloud radars, Meteorological Monographs, 57, 17.11-17.19, 2016.

Kollias, Puigdomènech Treserras, B., and Protat, A.: Calibration of the 2007–2017 record of Atmospheric Radiation Measurements cloud radar observations using CloudSat, Atmospheric Measurement Techniques, 12, 4949-4964, 2019.

Laird, N. F., Ochs Iii, H. T., Rauber, R. M., and Miller, L. J.: Initial precipitation formation in warm Florida cumulus, Journal of the atmospheric sciences, 57, 3740-3751, 2000.

Leon, D. C., Wang, Z., and Liu, D.: Climatology of drizzle in marine boundary layer clouds based on 1 year of data from CloudSat and Cloud‑Aerosol Lidar and Infrared Pathfinder Satellite Observations (CALIPSO), Journal of Geophysical Research: Atmospheres, 113, 2008.

Liu, Y., Geerts, B., Miller, M., Daum, P., and McGraw, R.: Threshold radar reflectivity for drizzling clouds, Geophysical research letters, 35, 2008.

Luke, E. P., and Kollias, P.: Separating Cloud and Drizzle Radar Moments during Precipitation Onset Using Doppler Spectra, Journal of Atmospheric and Oceanic Technology, 30, 1656-1671, 10.1175/jtech-d-11-00195.1, 2013.

Ma, Y., and Guo, G.: Support vector machines applications, Springer, 2014.

Mace, G. G., Protat, A., Humphries, R. S., Alexander, S. P., McRobert, I. M., Ward, J., Selleck, P., Keywood, M., and McFarquhar, G. M.: Southern Ocean cloud properties derived from CAPRICORN and MARCUS data, Journal of Geophysical Research: Atmospheres, 126, e2020JD033368, 2021.

Michibata, T., and Suzuki, K.: Reconciling compensating errors between precipitation constraints and the energy budget in a climate model, Geophysical Research Letters, 47, e2020GL088340, 2020.

Nicholls, S.: The dynamics of stratocumulus: Aircraft observations and comparisons with a mixed layer model, Quarterly Journal of the Royal Meteorological Society, 110, 783-820, 1984.

Paluch, I., and Lenschow, D.: Stratiform cloud formation in the marine boundary layer, Journal of the atmospheric sciences, 48, 2141-2158, 1991.

Randall, D. A., Coakley, J. A., Fairall, C. W., Kropfli, R. A., and Lenschow, D. H.: OUTLOOK FOR RESEARCH ON SUB-TROPICAL MARINE STRATIFORM CLOUDS, Bulletin of the American Meteorological Society, 65, 1290-1301, 10.1175/1520-0477(1984)065<1290:ofrosm>2.0.co;2, 1984.

Stephens, G. L.: Cloud feedbacks in the climate system: A critical review, Journal of climate, 18, 237-273, 2005.

Takahashi, H., Suzuki, K., and Stephens, G.: Land–ocean differences in the warm-rain formation process in satellite and ground-based observations and model simulations, Quarterly Journal of the Royal Meteorological Society, 143, 1804-1815, 2017.

VanZanten, M., Stevens, B., Vali, G., and Lenschow, D.: Observations of drizzle in nocturnal marine stratocumulus, Journal of the atmospheric sciences, 62, 88-106, 2005.

Vapnik, V., Golowich, S. E., and Smola, A.: Support vector method for function approximation, regression estimation, and signal processing, Advances in neural information processing systems, 281-287, 1997.

Vial, J., Dufresne, J.-L., and Bony, S.: On the interpretation of inter-model spread in CMIP5 climate sensitivity estimates, Climate Dynamics, 41, 3339-3362, 2013.

Wang, H., and Feingold, G.: Modeling mesoscale cellular structures and drizzle in marine stratocumulus. Part I: Impact of drizzle on the formation and evolution of open cells, Journal of the Atmospheric Sciences, 66, 3237-3256, 2009.

Wang, J., Dong, X., and Wood, R.: Aerosol and Cloud Experiments in Eastern North Atlantic (ACE-ENA) Science Plan, DOE Office of Science Atmospheric Radiation Measurement (ARM) Program …, 2016.

Warren, S., Hahn, C., London, J., Chervin, R., and Jenne, R.: Global distribution of total cloud cover and cloud types over land. NCAR Tech, Note NCAR/TN-273+ STR, 29 pp.+ 200 maps, Natl. Cent. for Atmos. Res …, 1986.

Warren, S., Hahn, C., London, J., Chervin, R., and Jenne, R.: Global distribution of total cloud cover and cloud types over ocean. NCAR Tech, Note NCAR/TN-317+ STR, 42 pp.+ 170 maps, 1988.

Wood: Drizzle in stratiform boundary layer clouds. Part 1: Vertical and horizontal structure, Journal of the Atmospheric Sciences, 62, 3011-3033, 10.1175/jas3529.1, 2005a.

Wood: Stratocumulus Clouds, Monthly Weather Review, 140, 2373-2423, 10.1175/mwr-d-11-00121.1, 2012.

577 Wood, R.: Drizzle in stratiform boundary layer clouds. Part II: Microphysical aspects, Journal of
578 the Atmospheric Sciences, 62, 3034-3050, 10.1175/jas3530.1, 2005b.
579 Wood, R.: Rate of loss of cloud droplets by coalescence in warm clouds, Journal of Geophysical
580 Research: Atmospheres, 111, 2006.
581 Wu, Dong, X., and Xi, B.: Marine boundary layer drizzle properties and their impact on cloud
582 property retrieval, Atmospheric Measurement Techniques, 8, 3555-3562, 10.5194/amt-8-3555-
583 2015, 2015.
584 Yamaguchi, T., Feingold, G., and Kazil, J.: Stratocumulus to cumulus transition by drizzle, Journal
585 of Advances in Modeling Earth Systems, 9, 2333-2349, 2017.
586 Yang, F., Luke, E. P., Kollias, P., Kostinski, A. B., and Vogelmann, A. M.: Scaling of drizzle virga
587 depth with cloud thickness for marine stratocumulus clouds, Geophysical Research Letters, 45,
588 3746-3753, 2018.
589 Zhang, Z., Song, Q., Mechem, D. B., Larson, V. E., Wang, J., Liu, Y., Witte, M. K., Dong, X., and Wu,
590 P.: Vertical dependence of horizontal variation of cloud microphysics: observations from the ACE-
591 ENA field campaign and implications for warm-rain simulation in climate models, Atmospheric
592 Chemistry and Physics, 21, 3103-3121, 2021.
593 Zhou, X., Kollias, P., and Lewis, E. R.: Clouds, precipitation, and marine boundary layer structure
594 during the MAGIC field campaign, Journal of Climate, 28, 2420-2442, 2015.
595 Zhu, Z., Kollias, P., Yang, F., and Luke, E.: On the estimation of in‐cloud vertical air motion using
596 radar Doppler spectra, Geophysical Research Letters, 48, e2020GL090682, 2021.
597
598
599
600

601   Figures and Tables:
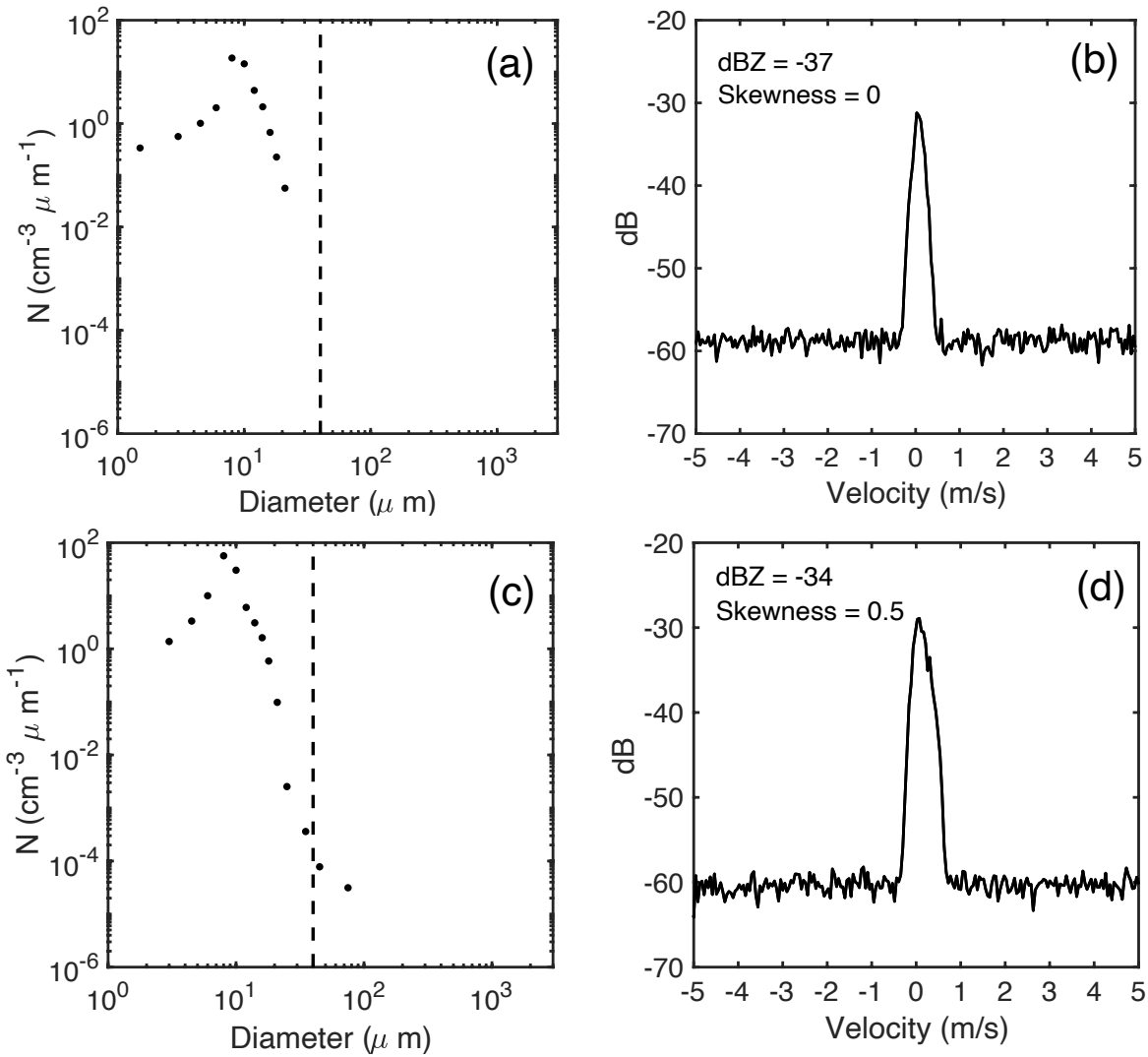
602

603   Figure 1: In-situ observed DSD of cloud-only (a) and the corresponding simulated Doppler Radar
604   spectrum (b), reflectivity and skewness of the spectrum are indicated in the upper left corner. (c)
605   and (d) are same as (a), (b) but for mixed cloud-drizzle DSD. The dash line in (a), (c) indicates
606   diameter with 40 μm.

607

608

609

610

611

612

613

614

615
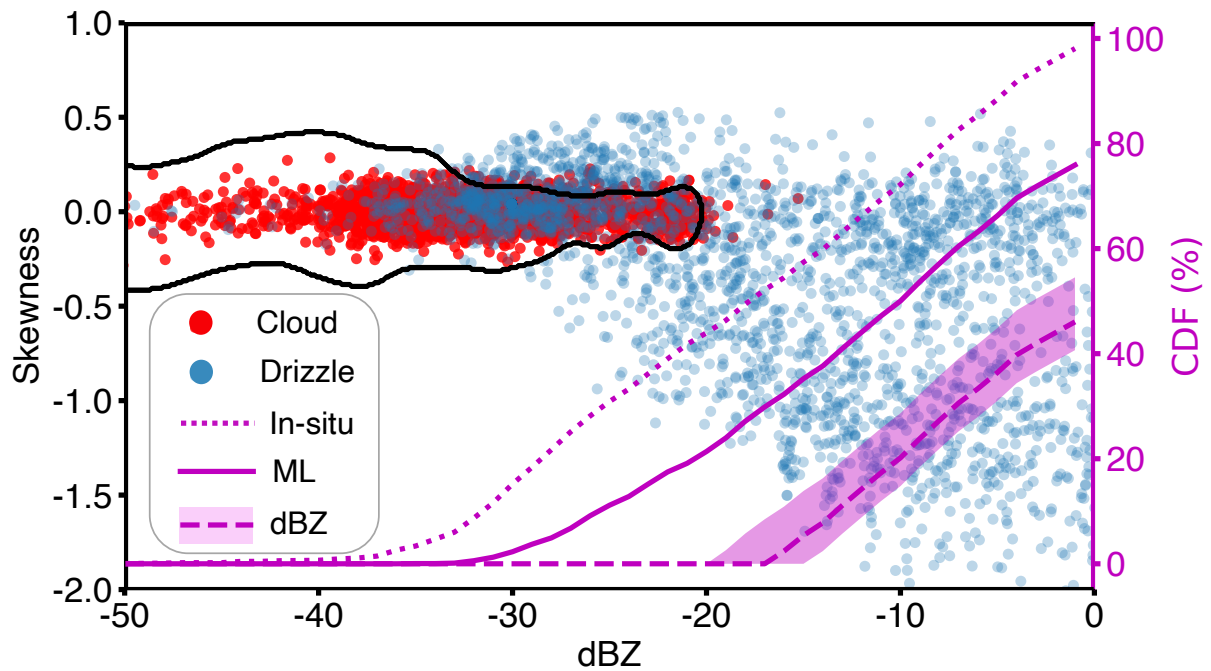
Figure 2: Distribution of the cloud-only (red points) and mixed cloud-drizzle (blue points) samples from the in-situ observation over the reflectivity-skewness space. The black line indicates the classification boundary of cloud/drizzle resolved by Machine Learning algorithm. Right axis indicates the CDF of all correctly identified drizzly samples as a function of reflectivity by each method: dotted magenta line is for the in-situ observations, which represents the true value; solid magenta line is for the ML technique; the magenta shading is for the reflectivity-based technique with upper boundary using dBZ > -20 and lower boundary using dBZ > -15; the dashed magenta line is for the reflectivity-threshold technique with dBZ > -17.

624

625

626

627

628

629

630

631

632

633

634 Table 1: Precision(P) and Recall(R) of the drizzle/cloud classification outcome for different
635 combination of C and Γ. The dark shaded cell represents the classification performance for the
636 selected parameters (C=1, Γ=50) being used in the study.
637

Γ C	1	10	50	100	200	500
1	0.99(P)	0.98(P)	0.98(P)	0.98(P)	0.97(P)	0.92(P)
	0.82(R)	0.85(R)	0.85(R)	0.85(R)	0.86(R)	0.87(R)
10	0.99(P)	0.98(P)	0.98(P)	0.98(P)	0.94(P)	0.91(P)
	0.84(R)	0.85(R)	0.85(R)	0.85(R)	0.85(R)	0.86(R)
50	0.99(P)	0.98(P)	0.98(P)	0.97(P)	0.93(P)	0.89(P)
	0.84(R)	0.85(R)	0.85(R)	0.85(R)	0.86(R)	0.87(R)
100	0.99(P)	0.98(P)	0.98(P)	0.96(P)	0.92(P)	0.89(P)
	0.84(R)	0.85(R)	0.84(R)	0.85(R)	0.86(R)	0.87(R)
200	0.98(P)	0.98(P)	0.98(P)	0.95(P)	0.91(P)	0.89(P)
	0.85(R)	0.84(R)	0.84(R)	0.85(R)	0.86(R)	0.87(R)
500	0.98(P)	0.98(P)	0.98(P)	0.94(P)	0.91(P)	0.88(P)
	0.85(R)	0.84(R)	0.85(R)	0.86(R)	0.86(R)	0.87(R)
1000	0.98(P)	0.98(P)	0.97(P)	0.94(P)	0.90(P)	0.88(P)
	0.85(R)	0.84(R)	0.84(R)	0.86(R)	0.86(R)	0.88(R)

638
639
640
641
642
643
644
645
646
647
648

649

650
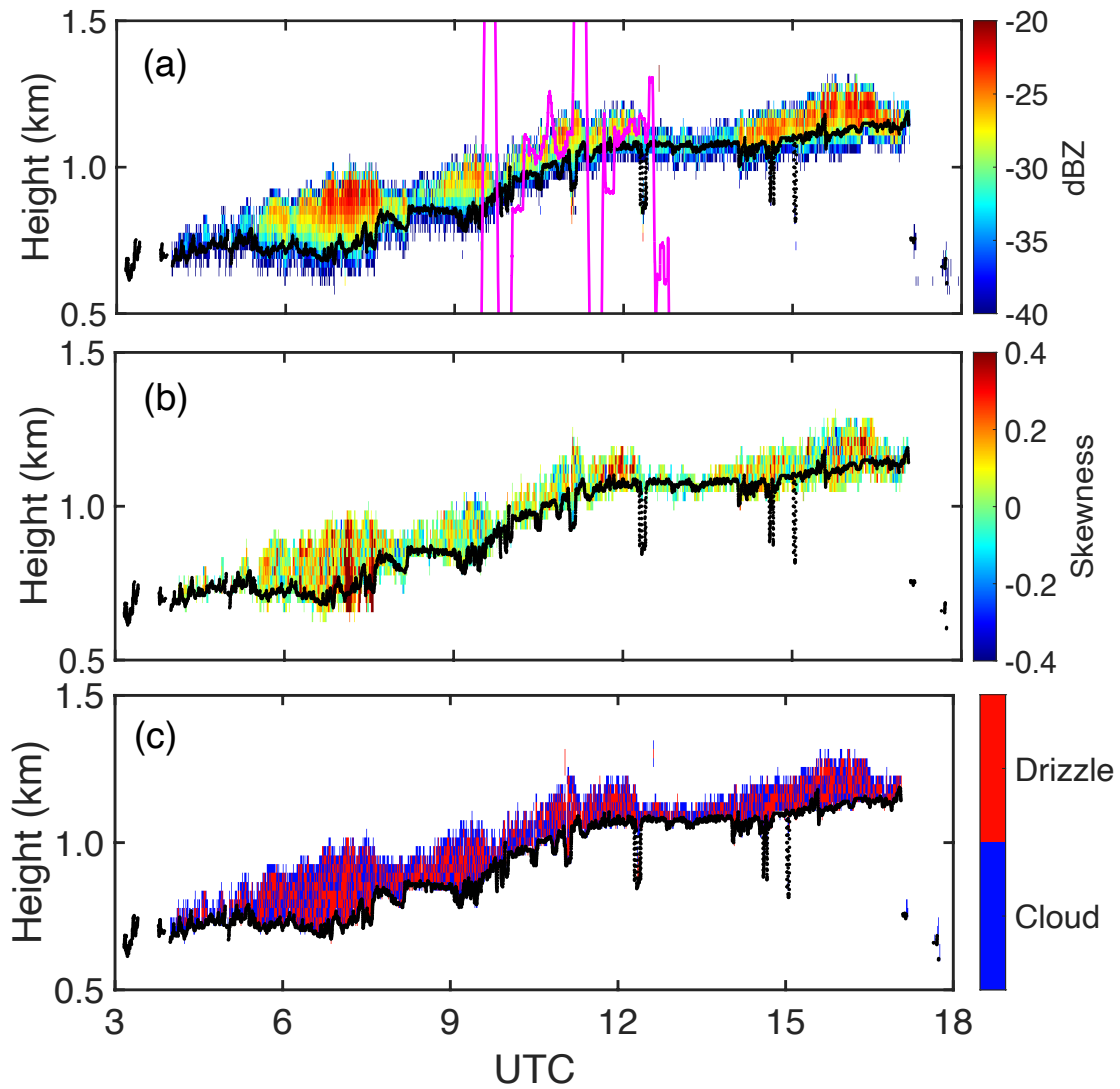
Figure 3: Reflectivity (a), skewness (b) and the classification mask (c) on June 30, 2017, at ENA site. Black line indicates the ceilometer-determined cloud base, magenta line in (a) indicates altitude track of the aircraft during the observation period.

654

655

656

657

658

659
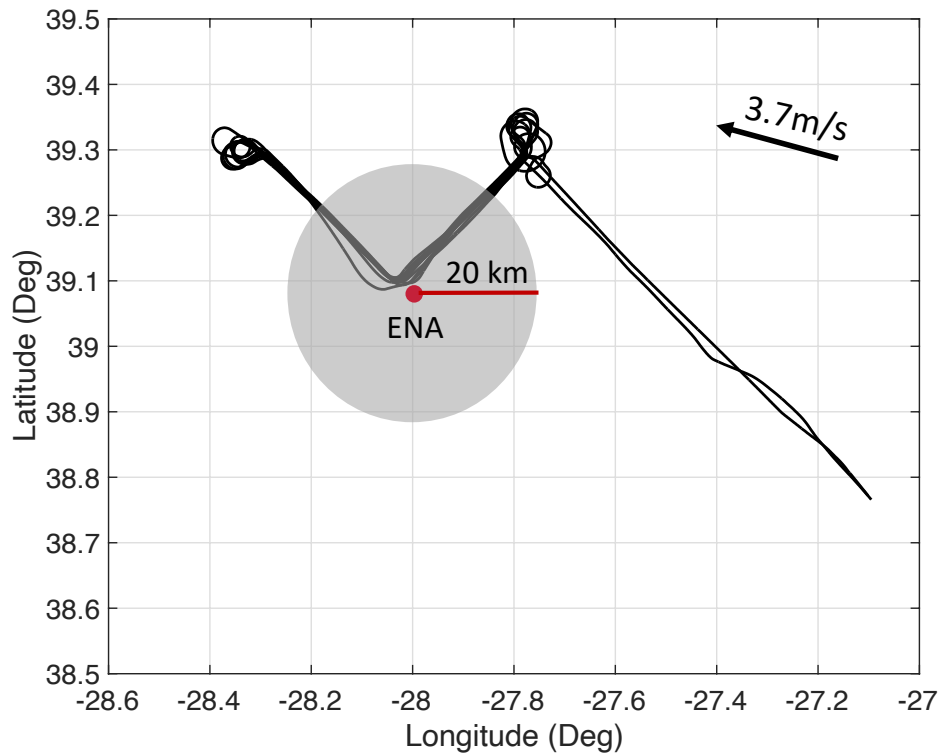
Figure 4: Aircraft track (black line) during the operational period on June 30, 2017. Shaded circle indicates the area within 20km around ENA site. The arrow in the upper right corner indicates mean wind direction and wind velocity in cloud layer during the observational period.

663

664

665

666

667

668

669

670

671

672

673

674

675

676

677

678

679 Table 2: Selected stratocumulus days in ACE-ENA, MAGIC and MARCUS campaigns.

ARM site	Selected Days
ENA	20170603, 20170604, 20170605, 20170616, 20170617, 20170627,20170628, 20170630, 20170701,20170702, 20160703, 20170706, 20170707, 20170709, 20170713,20170714, 20170715, 20170718, 20170719
MAGIC	20121016, 20121020, 20121030, 20121105, 20130526, 20130604,20130605, 20130708, 20130709, 20130710, 20130717, 20130720, 20130721,20130722, 20130729, 20130730, 20130731, 20130804
MARCUS	20180109, 20180110 ,20180228, 20180301, 20180322, 20180323

680

681

682

683

684

685

686

687

688

689
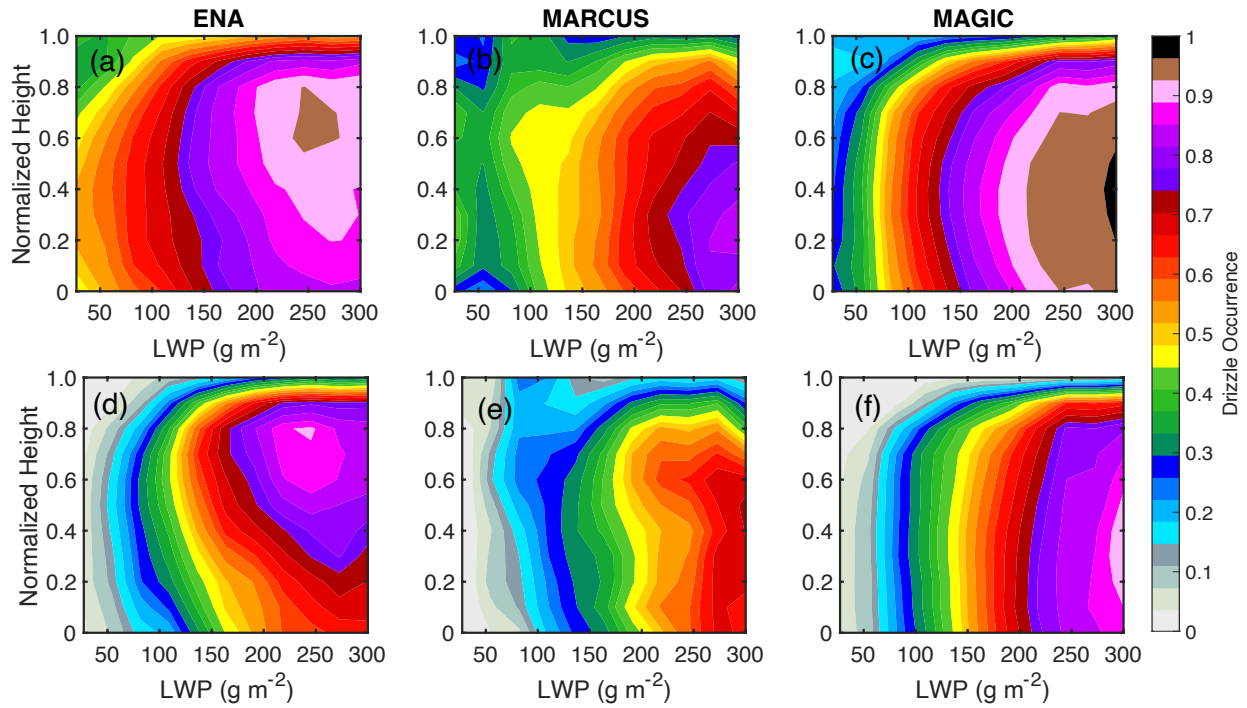
Figure 5: Vertical distribution of drizzle occurrence categorized by LWP based on MLA under ENA (a), MARCUS (b) and MAGIC (c) observational campaigns. (d), (e) and (f) are same as (a), (b), (c) except the drizzle is detected by dBZA.
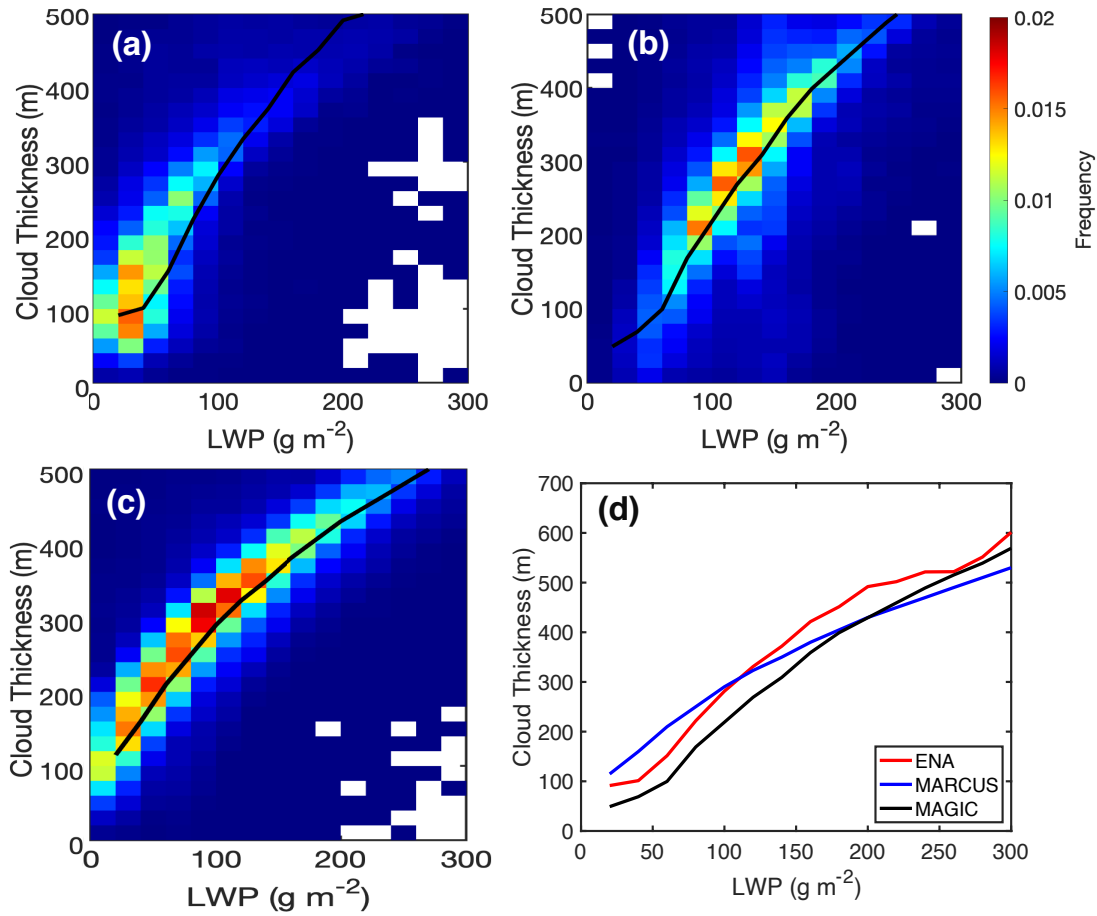
Figure 6: Joint histogram of cloud thickness and LWP at three campaigns: (a) ENA, (b) MARCUS and (c) MAGIC. The black line indicates the mean cloud thickness in each LWP category. For comparison, the relationship between mean cloud thickness and LWP at three campaigns (black line in (a),(b),(c)) are shown in (d).

715
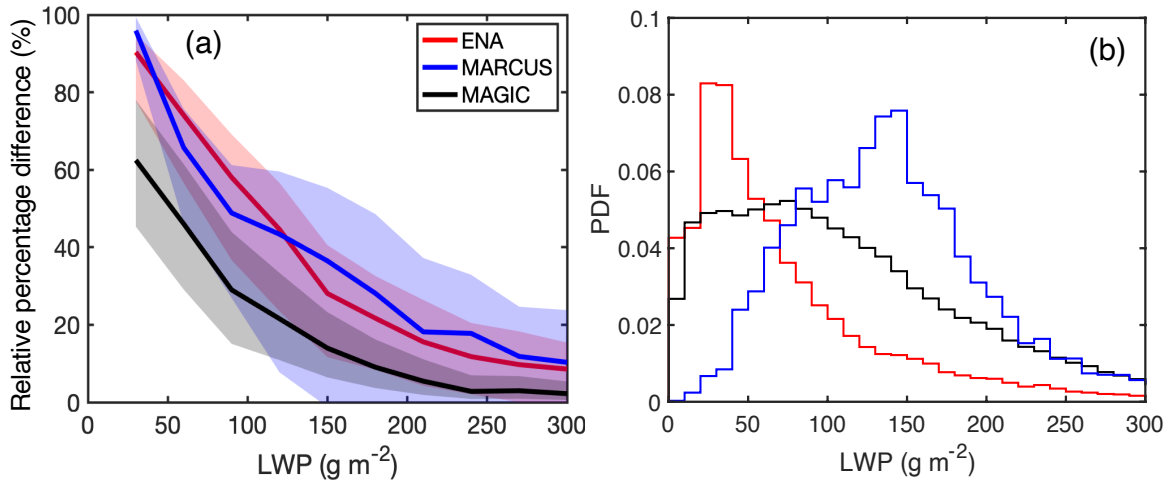
Figure 7: (a) Relative percentage difference of drizzle detection between the dBZA (dBZ > -17) and MLA as a function of LWP at ARM observational campaigns: ENA (red line), MARCUS (blue line) and MAGIC (black line). The shading area indicates same results but with different reflectivity threshold being used: the upper boundary is for the dBZ > -15 and the lower boundary is for dBZ > -20. (b) Histogram of the LWP distribution collected at three campaigns: ENA (red line), MARCUS (blue line) and MAGIC (black line).

722
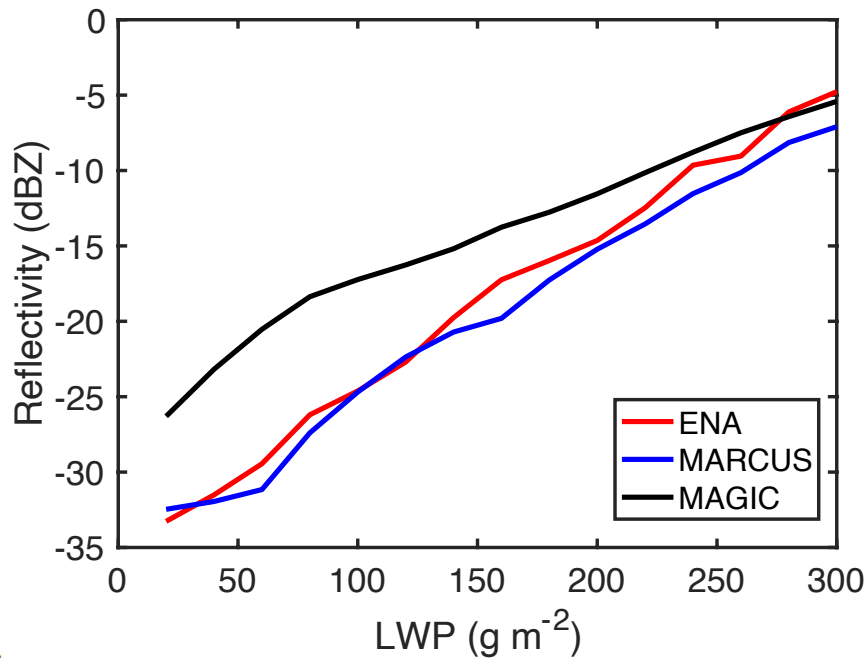
Figure 8: Mean KAZR reflectivity of the hydrometeor signal as a function of LWP at three campaigns: ENA (red line), MARCUS (blue line) and MAGIC (black line).

725